Spectral density of the two-impurity Anderson model

2006 J. Phys.: Condens. Matter 18 981

(http://iopscience.iop.org/0953-8984/18/3/015)

INSTITUTE OF PHYSICS PUBLISHING JOURNAL OF PHYSICS: CONDENSED MATTER

J. Phys.: Condens. Matter **18** (2006) 981–995 doi:10.1088/0953-8984/18/3/015

Spectral density of the two-impurity Anderson model

Satoshi Nishimoto[1], **Thomas Pruschke**[1] **and Reinhard M Noack**[2]

[1] Institut für Theoretische Physik, Universität Göttingen, D-37077 Göttingen, Germany
[2] Fachbereich Physik, Philipps-Universität Marburg, D-35032 Marburg, Germany

E-mail: nishimoto@theorie.physik.uni-goettingen.de

Received 4 November 2005
Published 6 January 2006
Online at stacks.iop.org/JPhysCM/18/981

Abstract

We investigate static and dynamical ground-state properties of the two-impurity Anderson model at half filling in the limit of vanishing impurity separation using the dynamical density-matrix renormalization group method. In the weak-coupling regime, we find a quantum phase transition as a function of inter-impurity hopping driven by the charge degrees of freedom. For large values of the local Coulomb repulsion, the transition is driven instead by a competition between local and non-local magnetic correlations. We find evidence that, in contrast to the usual phenomenological picture, it seems to be the bare effective exchange interactions which trigger the observed transition.

1. Introduction

Although 40 years have passed since the discovery of the Kondo effect, it is still one of the most interesting topics in condensed matter physics; it lies at the heart of understanding strongly correlated electron systems [1]. The Kondo effect, which leads to the quenching of an impurity spin, forms the basis of the physics of a single magnetic impurity embedded in a metal. However, systems with more than one impurity are considerably more complicated and present additional difficulties in a theoretical investigation. In particular, there are two effects which compete against each other in multiple-impurity systems: the Kondo effect and the Ruderman–Kittel–Kasuya–Yosida (RKKY) interaction. The RKKY exchange favours the formation of non-local magnetic correlations; the Kondo effect, on the other hand, is based on purely local magnetic correlations. The competition between the Kondo effect and the RKKY interaction is thought to be the key mechanism to understanding the magnetic properties of the heavy fermion materials [2]. The simplest systems which allow the study of this competition are two-impurity models. Recently, such models have also attracted much attention in the context of double quantum dots [3], which can be viewed as a direct experimental realization of the two-impurity Kondo model.

Theoretically, the two-impurity Anderson model (TIAM) [4–16] and the two-impurity Kondo model (TIKM) [17–34] have been extensively studied with various methods;

nevertheless, their physical properties at low temperature are not yet well understood. In particular, the situation is far from clear concerning dynamical properties because only a few methods are able to reliably calculate the dynamical properties of such models due to their complexity. So far, the spectral density has been calculated using perturbation theory (PT) [11, 14] and the numerical renormalization group (NRG) [22], but the results are not fully satisfactory. The PT provides an explicatory and accurate picture of quantum impurity dynamics only in certain limiting cases. While the NRG can determine the low-energy dynamics of quantum impurity models almost exactly, it is less precise at high energy.

Recently, the dynamical density-matrix renormalization group (DDMRG) method [35] was applied to the single-impurity Anderson model (SIAM) and it was shown that the method can calculate the impurity spectral density with good resolution for all frequencies and coupling strengths [36, 37]. This method can be extended to investigate the dynamics of a two-impurity problem without difficulty. Here we study the spectral density of the TIAM using the DDMRG method. Since the parameter space of the TIAM is rather large, for simplicity we focus here on the limit of small inter-impurity distance. This simplification does not change the substance of the problem and is quite likely relevant for typical experimental situations, e.g., clusters of magnetic atoms on metal surfaces or multiple-quantum-dot systems.

The aim of this paper is to demonstrate the efficiency of the DDMRG for the two-impurity system and to discuss the dynamical properties of the TIAM in the limit of zero impurity distance as the first step of a more general DDMRG study. The organization of this paper is as follows. In section 2, the model Hamiltonian for the TIAM is introduced. In section 3, we transform the Hamiltonian for an efficient treatment with the (D)DMRG and define even- and odd-parity orbitals of coupled impurities. In section 4, we show the static and the dynamic properties calculated with the (D)DMRG method. The conclusion and discussion follow in section 5.

2. Model

The Hamiltonian for two impurities placed at $\mathbf{R}_i$ $(i = 1, 2)$ is written as

$$\hat{H} = \sum_{\mathbf{k}\sigma} \varepsilon_{\mathbf{k}} \hat{f}^{\dagger}_{\mathbf{k}\sigma} \hat{f}_{\mathbf{k}\sigma} + \sum_{i\mathbf{k}\sigma} V_{\mathbf{k}} (\mathrm{e}^{\mathrm{i}\mathbf{k}\cdot\mathbf{R}_i} \hat{f}^{\dagger}_{\mathbf{k}\sigma} \hat{d}_{i\sigma} + \mathrm{h.c.}) + U \sum_{i=1,2} (\hat{n}^{d}_{i\uparrow} - \mu)(\hat{n}^{d}_{i\downarrow} - \mu) + t_{12} \sum_{\sigma} (\hat{d}^{\dagger}_{1\sigma} \hat{d}_{2\sigma} + \mathrm{h.c.}) \tag{1}$$

where $\hat{d}^{\dagger}_{i\sigma}$ $(\hat{d}_{i\sigma})$ creates (annihilates) an electron with spin $\sigma = \uparrow, \downarrow$ in a local level (the impurity site i), $\hat{n}^{d}_{i\sigma} = \hat{d}^{\dagger}_{i\sigma} \hat{d}_{i\sigma}$ and $\hat{f}^{\dagger}_{\mathbf{k}\sigma}$ $(\hat{f}_{\mathbf{k}\sigma})$ creates (annihilates) an electron with spin σ in an eigenstate of the (noninteracting) host band with dispersion $\varepsilon_{\mathbf{k}}$. The sum over $\mathbf{k}$ runs over all states of the host band. The hybridization between the local impurity state and the delocalized band state $\mathbf{k}$ is given by the positive couplings $V_{\mathbf{k}}$. Electrons in the local level are subject to a Coulomb repulsion U. In this paper, the energy level of impurity sites is set by $\mu = -U/2$. Under this assumption, we can map our model to the two-impurity Kondo model in the strong-coupling limit. We also set $\mathbf{R}_1 - \mathbf{R}_2 = \mathbf{0}$ and replace $\mathbf{k} \to k$ for simplicity. Thus, our model depends on the parameter U and the hybridization function

$$\Delta(\omega) = \pi \sum_{k} |V_k|^2 \delta(\omega - \varepsilon_k) \geqslant 0. \tag{2}$$

For a symmetric hybridization function, $\Delta(\omega) = \Delta(-\omega)$, the TIAM is particle–hole symmetric for $t_{12} = 0$.

Since, for the time being, we are interested in understanding the qualitative aspects of the model, it is convenient to choose a flat-band host density as the hybridization function.

In addition, the flat-band case of the SIAM is very well understood [1] and is thus helpful to explain features found in our model. We also take the host bandwidth to be much larger than any other bare energy scale and use a hybridization function which is constant, $\Delta(\omega) = \Delta_0$. Our goal is then to compute the spectral density in the relevant energy window $-W/2 < \omega < W/2$ with $W/2 > U/2, \Delta_0$. For all numerical results presented here, the energy scale is set by $\Delta_0 = 1/\pi$.

3. Method

In this work, we employ the DMRG technique [39], which is a reliable numerical method for one-dimensional systems. We use the standard DMRG method to calculate ground-state properties and the DDMRG method [35] to calculate dynamical properties. In order to carry out our calculations, we consider $N + 2$ electrons in a system consisting of N noninteracting bath sites (N even) and two impurity sites. The electron density is $\langle n_\uparrow \rangle = \langle n_\downarrow \rangle = N/2 + 1$.

The (D)DMRG calculations can be performed on finite lattices only, i.e., we must discretize the host band and carry out (D)DMRG calculations for a finite number N of host band eigenstates corresponding to energies ε_k ($k = 1, \ldots, N$), and then extrapolate the results to a continuous host band ($N \to \infty$) if needed. Choosing a discretization of the host band, i.e., selecting the N band state energies ε_k, should be done appropriately depending on what is to be obtained.

The Hamiltonian (1) is, however, somewhat unsuited for a DMRG treatment because it includes hopping terms that are long range. For example, the system size is limited to $N \leqslant 60$ for typical calculations even when several thousand density-matrix eigenstates are kept in the DMRG procedure, the maximum possible on current workstations. Therefore, we first transform the Hamiltonian (1) into a linear chain with nearest-neighbour hopping only,

$$\hat{H} = V \sum_{i\sigma} (\hat{c}^\dagger_{0\sigma} \hat{d}_{i\sigma} + \hat{d}^\dagger_\sigma \hat{c}_{0\sigma}) + \sum_{j\sigma} a_j \hat{c}^\dagger_{j\sigma} \hat{c}_{j\sigma} + \sum_{j\sigma} \lambda_j (\hat{c}^\dagger_{j\sigma} \hat{c}_{j+1\sigma} + \hat{c}^\dagger_{j+1\sigma} \hat{c}_{j\sigma}) + U \sum_{i=1,2} (\hat{n}^d_{i\uparrow} - \tfrac{1}{2})(\hat{n}^d_{i\downarrow} - \tfrac{1}{2}) + t_{12} \sum_\sigma (\hat{d}^\dagger_{1\sigma} \hat{d}_{2\sigma} + \text{h.c.}). \tag{3}$$

The new fermion operators $\hat{c}_{j\sigma}$ correspond to electronic states in the host band and are related to the original representation by a canonical transformation

$$\hat{c}_{j\sigma} = \sum_k M_{jk} \hat{f}_{k\sigma}. \tag{4}$$

The orthogonal matrix M_{jk}, the diagonal terms a_j, and the nearest-neighbour hopping terms λ_j are calculated using the Lanczos algorithm for tridiagonalizing a symmetric matrix starting from the initial vector $M_{1,k} = V_k/V$ with $V^2 = \sum_k V_k^2$. For a hybridization function (2) symmetric about $\omega = 0$, the diagonal terms a_j vanish. The Hamiltonian (3) describes two impurities coupled to one end of a one-dimensional chain representing the host band states (see figure 1). This transformation enables us to handle a system with up to $N \sim \mathcal{O}(200)$ bath states using the (D)DMRG method.

Furthermore, for efficient treatment, we introduce even- ($p = \text{e}$) and odd- ($p = \text{o}$) parity impurity orbitals $d_{\text{p}\sigma} = (d_{1\sigma} \pm d_{2\sigma})/\sqrt{2}$ as in [19]. With $\mathbf{R}_1 - \mathbf{R}_2 = \mathbf{0}$, the Hamiltonian (1) is transformed to

$$\hat{H} = \hat{H}_0 + \hat{H}_U \tag{5}$$

$$\hat{H}_0 = V \sum_\sigma (\hat{d}^\dagger_{\text{e}\sigma} \hat{c}_{0\sigma} + \text{h.c.}) + \sum_{j\sigma} \lambda_j (\hat{c}^\dagger_{j\sigma} \hat{c}_{j+1\sigma} + \text{h.c.}) + t_{12} \sum_\sigma (\hat{d}^\dagger_{\text{e}\sigma} \hat{d}_{\text{e}\sigma} - \hat{d}^\dagger_{\text{o}\sigma} \hat{d}_{\text{o}\sigma}) \tag{6}$$

$$\hat{H}_U = \frac{U}{2} [(\hat{n}_{\text{e}\uparrow} + \hat{n}_{\text{o}\uparrow} - 1)(\hat{n}_{\text{e}\downarrow} + \hat{n}_{\text{o}\downarrow} - 1) + (\hat{d}^\dagger_{\text{e}\uparrow} \hat{d}_{\text{o}\uparrow} + \hat{d}^\dagger_{\text{o}\uparrow} \hat{d}_{\text{e}\uparrow})(\hat{d}^\dagger_{\text{e}\downarrow} \hat{d}_{\text{o}\downarrow} + \hat{d}^\dagger_{\text{o}\downarrow} \hat{d}_{\text{e}\downarrow})], \tag{7}$$

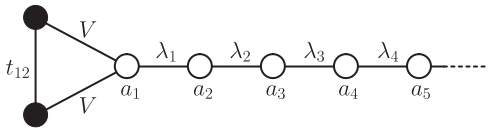

Figure 1. One-dimensional lattice configuration for applying the DMRG algorithm to the two-impurity problem. The solid circles denote the impurity sites and the open circles denote the host band.

where $\hat{n}_{\mathrm{e(o)}\sigma} = \hat{d}^{\dagger}_{\mathrm{e(o)}\sigma}\hat{d}_{\mathrm{e(o)}\sigma}$. Note that only the even-parity orbital hybridizes with the noninteracting bath states directly. When $U = 0$, the even- and odd-parity orbitals are completely separate. In our model, they will be mixed only via the Coulomb interaction.

4. Results

4.1. Static properties

We begin our discussion with some static properties of the system, namely, the electron density at the impurities and the spin–spin correlation function between the impurities, calculated with the standard DMRG method. Here we apply a logarithmic discretization scheme of the host band, $\varepsilon_k = (W/2)\Lambda^{-k}$ (with $\Lambda > 1$ and $k = 1, 2, \ldots, N/2$), as usually used in Wilson's renormalization group method [38], because we are interested in the case of large host bandwidth as well as in having dense bath states around the chemical potential for quantitative accuracy. Typically, we use $N = 38$ bath states with $\Lambda = 1.5$ and $W = 100\pi\Delta_0$ and keep $m = 2000$ density-matrix eigenstates in the DMRG procedure. In some cases, systems with up to $N = 58$ and $W = 1000\pi\Delta_0$ are used to extrapolate the results to $W \to \infty$.

4.1.1. Electron density at the impurity. The average electron densities $\langle\hat{n}_{\mathrm{e}}\rangle$ and $\langle\hat{n}_{\mathrm{o}}\rangle$ for even- and odd-parity orbitals of coupled impurities, respectively, are displayed in figures 2(a) and (b) for different values of U as a function of t_{12}. Since the two-impurity sites are equivalent, we have $\langle\hat{n}_1\rangle = \langle\hat{n}_2\rangle = \left(\langle\hat{n}_{\mathrm{e}}\rangle + \langle\hat{n}_{\mathrm{o}}\rangle\right)/2$. Note that $\langle\hat{n}_1\rangle\left(\langle\hat{n}_2\rangle\right)$ can take values between 0 and 2 due to the charge degrees of freedom at the impurity sites, in contrast to the two-impurity Kondo model for which $\langle\hat{n}_1\rangle = \langle\hat{n}_2\rangle = 1$ always.

When $t_{12} = 0$, $\langle\hat{n}_{\mathrm{e}}\rangle = \langle\hat{n}_{\mathrm{o}}\rangle = 1$ for all interaction strengths due to particle–hole symmetry. The local densities are drastically affected by t_{12}. We find a discontinuous transition at a critical value $t_{12} = t_{12,\mathrm{c}}$ which is dependent on U. The critical value $t_{12,\mathrm{c}}$ is zero at $U = 0$ and becomes larger with increasing U. In the large U limit, it saturates at $t_{12,\mathrm{c}} \sim \pi\Delta_0$. We show the critical value $t_{12,\mathrm{c}}$ as a function of U for $W \to \infty$ in the inset of figure 2(c).

At $U = 0$, $\langle\hat{n}_{\mathrm{o}}\rangle$ drops to zero for infinitesimally small t_{12} (<0). In this limit, there is no hybridization with the conduction band and no coupling to the even-parity level, i.e., the odd-parity orbital forms a completely local state at the Fermi level ε_{F} if $t_{12} = 0$. An infinitesimally small t_{12} shifts the state above ε_{F}, i.e., $t_{12,\mathrm{c}} = 0^{+}$. For small but finite U, the situation is similar and the transition is caused by the competition between t_{12} and U. At $t_{12} = 0$, the odd-parity orbital is split by the Coulomb interaction (see equation (7)) into two states with energy difference $\sim U/2$, the lower and the upper Hubbard band (we call them the LHB and the UHB, respectively) located at $\omega \approx \pm U/4$. A finite t_{12} has the effect of shifting the LHB to higher energies by $|t_{12}|$. The odd-parity orbital is occupied by one electron if the LHB is below ε_{F} and almost vacant if the LHB is above ε_{F}. This leads to $t_{12,\mathrm{c}} \sim U/4$ and a large discontinuity ($\sim$1) of $\langle\hat{n}_{\mathrm{o}}\rangle$ at $t_{12,\mathrm{c}}$. This anticipated behaviour is in fact observed in our DMRG

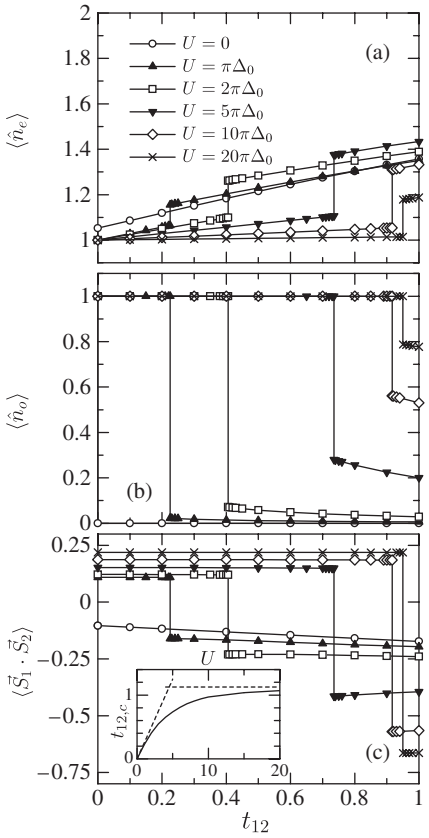

Figure 2. Local density on the even- (a) and odd- (b) parity orbitals of the coupled impurities as a function of t_{12} for several U values. (c) Spin–spin correlation function as a function of t_{12} and U. Inset: the critical values of the transition, $t_{12,c}$, as a function of U. The dashed lines correspond to $t_{12,c} = U/4$ and $t_{12,c} = 1.13$ (see text).

results. As U increases, the odd-parity orbital begins to hybridize indirectly with the host band via the interaction term (7). The discontinuity, therefore, becomes smaller and goes to zero as $U \to \infty$. Moreover, we find that $t_{12,c}$ has almost no U-dependence in the large-U regime. This implies that the physics behind the transition for large U is different from the competition between t_{12} and U at small U. Before we discuss a possible mechanism in the next paragraph, let us briefly comment on the behaviour of the even-parity orbital. For all U values, $\langle \hat{n}_e \rangle$ increases slowly as a function of t_{12} because the even-parity orbital hybridizes directly with the host band, thus experiencing a strong broadening. Hence, the discontinuity of $\langle \hat{n}_e \rangle$ at $t_{12} = t_{12,c}$ is smaller than that of $\langle \hat{n}_o \rangle$. We can also see the largest discontinuity, which means that the charge fluctuation on the even-parity orbital is largest, for intermediate U values ($U \sim 5\pi\Delta_0$). We also note that $\langle \hat{n}_o \rangle = 1$ independent of U below $t_{12,c}$, and $\langle \hat{n}_o \rangle \to 0$ and $\langle \hat{n}_e \rangle \to 2$ as $t_{12} \to \infty$ for finite U.

4.1.2. Spin–spin correlation between impurities. We now investigate the spin–spin correlation between the two impurities, $\langle \vec{S}_1 \cdot \vec{S}_2 \rangle$. The results are shown in figure 2(c) as a function of t_{12} for different values of U. Before we discuss the results, let us first identify the different types of magnetic interactions present in our model. First, we have the c–f exchange

interaction $J_{\rm cf}$, which is the antiferromagnetic interaction between an electron on the impurity sites and conduction electrons. For a single impurity, $J_{\rm cf}$ leads to the Kondo effect and a *local* spin singlet as the ground state. Within the standard Schrieffer–Wolff mapping, the value for $J_{\rm cf}$ is given by $J_{\rm cf} = 8\Delta_0/U_{\rm eff}$, where $U_{\rm eff}$ is the effective Coulomb interaction and the impurities are both occupied by one electron. The c–f exchange is effective only when an electron is localized on the impurity so that $U_{\rm eff} = U/2$ and $J_{\rm cf} = 16\Delta_0/U$. Second, the conduction electrons mediate the RKKY interaction $J_{\rm RKKY}$. For our particular set-up, we obtain a ferromagnetic interaction between two electrons on the impurity sites. As usual, $J_{\rm RKKY}$ is obtained as second-order process, i.e., $J_{\rm RKKY} \sim J_{\rm cf}^2 \sim \mathcal{O}(1/U^2)$. Third, the model exhibits a direct exchange interaction $J_{\rm ex}$ due to the coupling t_{12}, which is an antiferromagnetic interaction and is given by the standard expression $J_{\rm ex} = 4t_{12}^2/U$.

We expect that for $t_{12} < t_{12,\rm c}$ ferromagnetic correlations due to the RKKY interaction are dominant, i.e., $\langle \vec{S}_1 \cdot \vec{S}_2 \rangle > 0$. On the other hand, when $t_{12} > t_{12,\rm c}$, antiferromagnetic correlations due to the exchange interaction are stronger, i.e., $\langle \vec{S}_1 \cdot \vec{S}_2 \rangle < 0$. Such a transition from ferromagnetic to antiferromagnetic correlations at $t_{12,\rm c}$ is in fact found at all interaction strengths, as can be seen in figure 2(c). The absolute value of $\langle \vec{S}_1 \cdot \vec{S}_2 \rangle$ increases with increasing U and reaches the maximum possible value as $U \to \infty$, which means that one electron is localized on each impurity in the $U \to \infty$ limit.

Let us now consider the U-dependence of the critical value $t_{12,\rm c}$. The transition is driven by the charge degrees of freedom in the weak-coupling regime. However, the spin degrees of freedom play an essential role in the strong-coupling regime. Taking into account that the spin–spin correlations between the impurity sites change from ferromagnetic to antiferromagnetic at $t_{12,\rm c}$, we may expect that the competition between the RKKY and direct exchange interactions is the origin of the transition. If we take $J_{\rm ex} = J_{\rm RKKY}$ as the criterion for the occurrence of the transition, we obtain $t_{12,\rm c} \sim \mathcal{O}(1/\sqrt{U})$. Thus, $t_{12,\rm c}$ would go to zero as $U \to \infty$, which is obviously inconsistent with the DMRG results, which show almost constant $t_{12,\rm c}$ as a function of U.

Up to now, we have not taken into account $J_{\rm cf}$, which leads to a competition between the formation of local Kondo and non-local singlets, offering a quite different mechanism for the transition. In this case, the criterion to obtain $t_{12,\rm c}$ is $J_{\rm cf} = J_{\rm ex}$, which gives $t_{12,\rm c} = \sqrt{4/\pi} \sim 1.13$. This result is indeed consistent with our findings. Thus, the transition in the strong-coupling regime can be interpreted as competition between local singlet formation due to the Kondo effect and non-local singlet formation due to the direct exchange introduced by t_{12}. Note, however, that, in contrast to the general folklore, the boundary is *not* set by $T_{\rm K}(J_{\rm cf}) = J_{\rm ex}$, but by the direct comparison of the bare energy scales. We also find that the total spin is $S = 1$ for $t_{12} < t_{12,\rm c}$ and $S = 0$ for $t_{12} > t_{12,\rm c}$.

4.2. Dynamical properties

In this section, we study the spectral density for impurities in the TIAM. The impurity one-particle Green function for even- and odd-parity orbitals can be written as

$$G_{{\rm p}\sigma}(\omega) = \left\langle \hat{d}_{{\rm p}\sigma}^{\dagger} \frac{1}{\hat{H} - E_0 + \omega - {\rm i}\eta} \hat{d}_{{\rm p}\sigma} \right\rangle + \left\langle \hat{d}_{{\rm p}\sigma} \frac{1}{E_0 - \hat{H} + \omega + {\rm i}\eta} \hat{d}_{{\rm p}\sigma}^{\dagger} \right\rangle \tag{8}$$

($\eta \to 0^+$), where E_0 is the ground-state energy and $\langle \cdots \rangle$ represents a ground-state expectation value. The impurity spectral density for each parity is then obtained as

$$D_{{\rm p}\sigma}(\omega) = -\frac{1}{\pi} {\rm sgn}(\omega)\, {\rm Im}\, G_{{\rm p}\sigma}(\omega) = A_{{\rm p}\sigma}(\omega) + B_{{\rm p}\sigma}(\omega) \tag{9}$$

with

$$A_{\mathrm{p}\sigma}(\omega \leqslant 0) = \lim_{\eta\to 0}\left\langle \hat{d}^{\dagger}_{\mathrm{p}\sigma}\frac{\eta}{\pi[(\hat{H}-E_0+\omega)^2+\eta^2]}\hat{d}_{\mathrm{p}\sigma}\right\rangle \tag{10}$$

$$B_{\mathrm{p}\sigma}(\omega \geqslant 0) = \lim_{\eta\to 0}\left\langle \hat{d}_{\mathrm{p}\sigma}\frac{\eta}{\pi[(\hat{H}-E_0-\omega)^2+\eta^2]}\hat{d}^{\dagger}_{\mathrm{p}\sigma}\right\rangle \tag{11}$$

and $A_{\mathrm{p}\sigma}(\omega \geqslant 0) = B_{\mathrm{p}\sigma}(\omega \leqslant 0) = 0$. The spectral density fulfils the sum rule

$$\int_{-\infty}^{\infty} D_{\mathrm{p}\sigma}(\omega)\,\mathrm{d}\omega = 1. \tag{12}$$

Note that the spectral densities for both impurities are the same, i.e., $D_{1\sigma}(\omega) = D_{2\sigma}(\omega)$, and are equal to $[D_{\mathrm{o}\sigma}(\omega) + D_{\mathrm{e}\sigma}(\omega)]/2$.

The standard DMRG algorithm [39, 40] can be used to calculate the ground-state properties as shown in the last section. In particular, the ground-state wavefunction $|\Psi_0\rangle$ and the ground-state energy E_0 can readily be obtained. To compute dynamic properties such as the impurity Green's function (8) we use the DDMRG [35]. This approach is based on a variational principle. One can easily show that for $\eta > 0$ and fixed frequency ω the minimum of the functional

$$W(\Psi) = \langle\Psi|(E_0+\omega-\hat{H})^2+\eta^2|\Psi\rangle + \eta\langle\Psi_0|\hat{d}_{\mathrm{p}\sigma}|\Psi\rangle + \eta\langle\Psi|\hat{d}^{\dagger}_{\mathrm{p}\sigma}|\Psi_0\rangle \tag{13}$$

with respect to all quantum states $|\Psi\rangle$ is

$$W(\Psi_{\min}) = \langle\Psi_0|\hat{d}_{\mathrm{p}\sigma}\frac{-\eta^2}{(E_0+\omega-\hat{H})^2+\eta^2}\hat{d}^{\dagger}_{\mathrm{p}\sigma}|\Psi_0\rangle. \tag{14}$$

The functional minimum is related to the convolution of the spectral density (11) with a Lorentz distribution of width η by

$$W(\Psi_{\min}) = -\pi\eta B^{\eta}_{\mathrm{p}\sigma}(\omega). \tag{15}$$

A similar result is obtained for the spectral density (10) if one substitutes $\hat{d}_{\mathrm{p}\sigma}$ for $\hat{d}^{\dagger}_{\mathrm{p}\sigma}$, $-\omega$ for ω and $A^{\eta}_{\mathrm{p}\sigma}(\omega)$ for $B^{\eta}_{\mathrm{p}\sigma}(\omega)$ in the above equations.

The DDMRG method consists essentially of minimizing the functional (13) numerically using the standard DMRG algorithm. Thus, the DDMRG provides the spectral densities $A^{\eta}_{\mathrm{p}\sigma}(\omega)$ and $B^{\eta}_{\mathrm{p}\sigma}(\omega)$ for a finite broadening η. The full spectral density (9) convolved with the Lorentz distribution

$$D^{\eta}_{\mathrm{p}\sigma}(\omega) = \int_{-\infty}^{\infty}\mathrm{d}\omega'\, D_{\mathrm{p}\sigma}(\omega')\frac{\eta}{\pi[(\omega-\omega')^2+\eta^2]} \tag{16}$$

is given by the sum of $A^{\eta}_{\mathrm{p}\sigma}(\omega)$ and $B^{\eta}_{\mathrm{p}\sigma}(\omega)$. The real part of the Green's function can be calculated with no additional computational cost but is generally less accurate. The necessary broadening of spectral functions in DDMRG calculations is actually very useful for studying continuous spectra or for doing a finite-size scaling analysis [35].

What we really would like to obtain is the spectral density in the $\eta = 0$ limit. This can be done by carrying out a deconvolution of the DDMRG data [36]. In theory, a deconvolution amounts to solving (16) for $D_{\mathrm{p}\sigma}(\omega)$ using the DDMRG data on the left-hand side. We also know that the broadened spectral density of the impurity system on an infinite lattice ($N \to \infty$) is usually almost identical to the spectral density of the discretized impurity system ($N < \infty$) if $\eta \geqslant \Delta\varepsilon$. Therefore, one can make the approximation that the DDMRG data for $D^{\eta}_{\mathrm{p}\sigma}(\omega)$ describes the broadened spectral density for $N \to \infty$ and can then solve (16) approximately under the condition that $D_{\mathrm{p}\sigma}(\omega)$ is the exact spectral density of the TIAM. For instance, one can require that $D_{\mathrm{p}\sigma}(\omega)$ is a continuous and relatively smooth function. To obtain quantitatively accurate spectra after deconvolution, we need to take η smaller than the width of the spectra when $\eta = 0$.

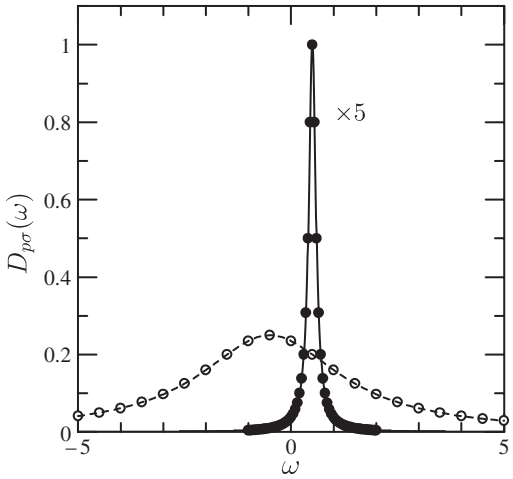

Figure 3. Spectral density at $U = 0$ and $W = 20\pi\Delta_0$. The open circles denote $D_{e\sigma}(\omega)$ calculated with a constant host band discretization for $N = 59$, $\Delta\varepsilon \approx 0.34\pi\Delta_0$, and $\eta = 0.5\pi\Delta_0$, then deconvolved. Solid circles denote $D_{e\sigma}(\omega)$ calculated with variable discretization $\Delta\varepsilon \approx 0.067\pi\Delta_0$ and $\eta = 0.1\pi\Delta_0$ around the peak. Solid and dashed lines are the exact solutions (17) with broadening $\eta = 0.1\pi\Delta_0$ and (18) without broadening, respectively.

4.2.1. Noninteracting case. The spectral density at $U = 0$ can be calculated exactly and provides a good test to demonstrate the accuracy of our method. The exact spectral density for the odd-parity orbital is a a δ-function at $\omega = -t_{12}$

$$D_{\rm o}(\omega) = \delta(\omega + t_{12}), \tag{17}$$

while for the even-parity orbital we obtain a Lorentzian of width $2\Delta_0$ centred at $\omega = t_{12}$

$$D_{\rm e}(\omega) = \frac{2\Delta_0}{\pi[(\omega - t_{12})^2 + (2\Delta_0)^2]}. \tag{18}$$

In figure 3, we show the spectral density calculated with the DDMRG for $U = 0$. On the scale of figure 3, there is no visible difference between our numerical results and the exact results. The deconvolution technique is not useful for obtaining a divergent function such as a δ-function, so we introduce a finite broadening $\eta = 0.1\pi\Delta_0$ into equation (17) and compare it to our 'bare' DDMRG spectra convolved with same η. Note that the local Coulomb interaction U is always treated numerically exactly in the density-matrix renormalization and thus does not affect the accuracy of the method directly.

4.2.2. Weak-coupling regime. In the weak-coupling regime ($U \ll 4\pi\Delta_0$), the physical properties are still similar to those of the noninteracting case. The spectral density of the impurities calculated with the DDMRG for $t_{12}/\Delta_0 = 0$, 0.15π, and 0.25π at $U = \pi\Delta_0$ is shown in figure 4. The critical coupling $t_{12,c}$ is $0.205\pi\Delta_0$. Let us first look at the spectrum for the even-parity orbital, $D_{e\sigma}(\omega)$. At $t_{12} = 0$ (see figure 4(a)), $D_{e\sigma}(\omega)$ is basically a Lorentzian of width $\sim 2\Delta_0$ centred at $\omega = 0$, but there appear small shoulders around $\omega \sim \pm 0.8\pi\Delta_0 (\sim U)$ and $\omega \sim \pm 1.8\pi\Delta_0 (\sim 2U)$ due to the Coulomb interaction (7). When t_{12} increases, the central peak is shifted towards lower energies by $|t_{12}|$ while maintaining its shape (see figures 4(b) and (c)). This is consistent with the gradual increase of the local density on the even-parity orbital $\langle \hat{n}_{\rm e} \rangle$ as a function of t_{12} and also with the small discontinuity at $t_{12,c}$, as shown in figure 2(a). We next turn to the spectrum for the odd-parity orbital, $D_{o\sigma}(\omega)$. As long as

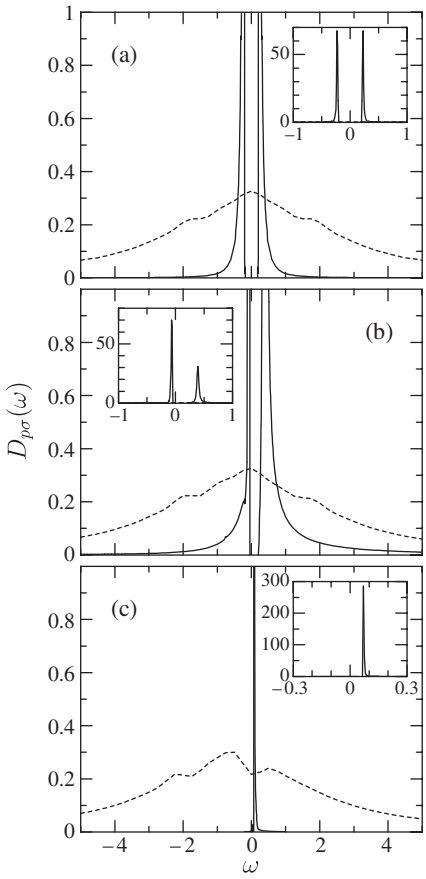

Figure 4. Spectral density of the coupled impurities for the odd-parity orbital $D_{o\sigma}(\omega)$ and for the even-parity orbital $D_{e\sigma}(\omega)$ with (a) $t_{12} = 0$, (b) $t_{12} = 0.15\pi\Delta_0$, and (c) $t_{12} = 0.25\pi\Delta_0$ at $U = \pi\Delta_0$ and $W = 20\pi\Delta_0$. Dashed lines denote $D_{e\sigma}(\omega)$ calculated with a constant host band discretization for $N = 58$, $\Delta\varepsilon \approx 0.34\pi\Delta_0$, and $\eta = 0.5\pi\Delta_0$, then deconvolved. Solid lines denote $D_{o\sigma}(\omega)$ calculated with a variable discretization for $N = 118\,(N = 70)$, $0.01\pi \leqslant \Delta\varepsilon/\Delta_0 \leqslant 0.45\pi$ $(0.0033\pi \leqslant \Delta\varepsilon/\Delta_0 \leqslant 1.98\pi)$ and a constant broadening $\eta = 0.02\pi\Delta_0$ $(\eta = 0.005\pi\Delta_0)$ for $t_{12} = 0$ and $0.15\pi\Delta_0$ $(0.25\pi\Delta_0)$, then deconvolved. Insets: expanded view around the Fermi level $\omega = 0$.

$U = 0$, this orbital has no direct hybridization with the host band, so that $D_{o\sigma}(\omega)$ consists of a localized state, i.e., a single δ-function peak. When a small $U(\leqslant\pi\Delta_0)$ is introduced at $t_{12} = 0$, this peak splits into two peaks located around $\sim \pm U/4$ due to the effective repulsion on the odd-parity orbital $U_{\rm eff} = U/2$ (see equation (7)). They correspond to the LHB and the UHB. In other words, the odd-parity orbital is half filled and a Mott–Hubbard gap opens. The peaks are still very sharp but are no longer exact δ-functions, as we can see in figure 4(a), because the odd-parity orbital couples 'indirectly' to the host band via the even-parity orbital. As t_{12} increases, the two peaks are shifted towards higher energies by $|t_{12}|$, but their separation remains $\sim U/2$. The LHB and UHB become sharper (broader) while retaining their respective weights. In addition, no spectral weight is transferred to the gap. When the LHB reaches the Fermi level $\varepsilon_{\rm F}$ $(\omega = 0)$ at $t_{12} = t_{12,c}$ $(\sim U/4)$, the transition occurs. When $t_{12} > t_{12,c}$ (see figure 4(c)), only one peak is present, and it is above $\omega = 0$ and is very sharp. Actually, there must be some spectral weight below $\omega = 0$ because $\langle\hat{n}_o\rangle$ is not exactly zero (see figure 2(b)).

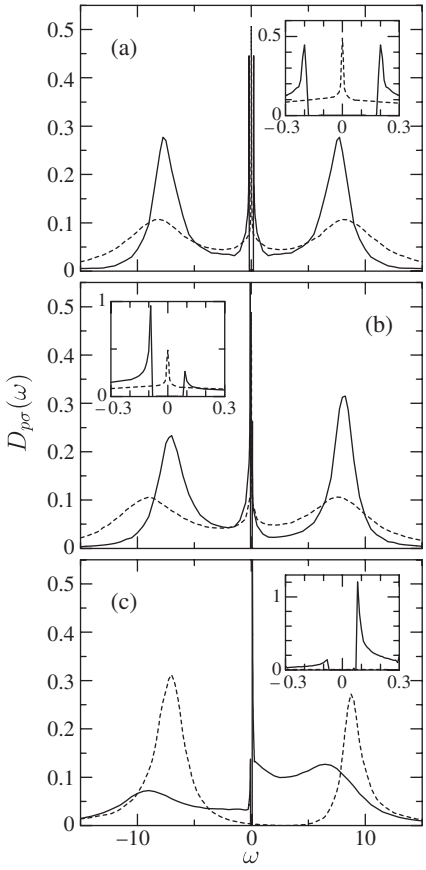

Figure 5. Spectral density of the coupled impurities for the odd-parity orbital $D_{o\sigma}(\omega)$ and for the even-parity orbital $D_{e\sigma}(\omega)$ with (a) $t_{12} = 0$, (b) $t_{12} = 0.6\pi\Delta_0$, and (c) $t_{12} = \pi\Delta_0$ at $U = 15\pi\Delta_0$ and $W = 40\pi\Delta_0$. Dashed lines denote $D_{e\sigma}(\omega)$ calculated with a variable discretization for $N = 94$, $\Delta\varepsilon \approx 0.0013\pi\Delta_0$, and $\eta = 0.002\pi\Delta_0$, then deconvolved. Solid lines denote $D_{o\sigma}(\omega)$ calculated with a variable discretization for $N = 94$, $0.0068\pi \leqslant \Delta\varepsilon/\Delta_0 \leqslant 1.98\pi$ and a constant broadening $\eta = 0.01\pi\Delta_0$, then deconvolved. Insets: expanded view around the Fermi level $\omega = 0$.

We therefore find that the odd-parity orbital behaves as a nearly localized state for all t_{12} and that the charge degrees of freedom in the odd-parity orbital play a crucial role for the transition.

4.2.3. Strong-coupling regime. We now consider the spectral density in the strong-coupling regime ($U \gg 4\pi\Delta_0$), which corresponds to the so-called Kondo regime in the SIAM. For the TIAM, however, the situation is more complex due to competing interactions, i.e., the RKKY interaction, the Kondo (or c–f exchange) effect, and the exchange interaction between impurity sites. In figure 5, we show the spectral density calculated with the DDMRG for $t_{12} = 0$, $0.6\pi\Delta_0$, and $\pi\Delta_0$ at $U = 15\pi\Delta_0$. The critical inter-impurity hopping $t_{12,c} \sim 0.8\pi\Delta_0$ is slightly smaller than that obtained in section 2 because the calculations were done for a finite host bandwidth here. Let us first look at the even-parity spectral density $D_{e\sigma}(\omega)$. Below $t_{12,c}$, we can see a sharp peak at $\omega = 0$ in $D_{e\sigma}(\omega)$, which satisfies the Friedel sum rule $D_{e\sigma}(\omega = 0) = 1/(2\pi\Delta_0)$. This means that the conduction electrons form a spin-singlet (Kondo) state with electrons in the even-parity orbital. The width of this peak at $\omega = 0$

becomes smaller exponentially with increasing U. We can thus state that the properties of $D_{e\sigma}(\omega)$ below $t_{12,c}$ are similar to that of the SIAM which is characterized by the Abrikosov–Suhl resonance at $\omega = 0$ and the Hubbard satellites around $\omega \approx \pm U/2$. Moreover, we notice that the physics of the TIAM is quite different from that of the two-impurity Kondo model, where no Kondo effect is observed [32], at least for the case of equivalent impurities. Note also that in the TIAM states with only one electron on the two impurity sites can still have a large weight ($\sim$3% for $U = 15\pi\Delta_0$) in the eigenvector of the ground-state even in the Kondo regime, in contrast to the two-impurity Kondo model.

When we increase t_{12}, the shape of $D_{e\sigma}(\omega)$ is hardly changed and only a weak transfer of spectral weight from above ε_F to below ε_F occurs, consistent with the behaviour of $\langle \hat{n}_e \rangle$. As long as t_{12} is smaller than $t_{12,c}$, the quasi-particle peak stays pinned at $\omega = 0$ and maintains its height $(1/(\pi\Delta_0))$, while the Hubbard satellites stay located at $|\omega| < U/2$ with width $>2\Delta_0$. Above $t_{12,c}$, on the other hand, the Kondo peak vanishes. The local spin is now screened due to the formation of a non-local singlet between the impurities due to the dominant exchange interaction; i.e., the scattering channels leading to the Abrikosov–Suhl resonance are not active any more. Simultaneously, the 'effective' hybridization between the host band and the even-parity orbital becomes weaker so that the width of the Hubbard satellites becomes narrower. Our numerical results indicate that the Hubbard satellites turn into Lorentzians with width $2\Delta_0$ and weight $1/2$ located at $|\omega| = U/2$ in the limit of $t_{12} \to \infty$ and $U \to \infty$.

Next, let us turn to the odd-parity spectral density $D_{o\sigma}(\omega)$. At $t_{12} = 0$, we find four peaks. The two prominent peaks located at $\omega \approx \pm 7.5$ $(= \pm\,\pi\Delta_0 U/2)$ can be identified with the Hubbard bands of the electrons localized in this orbital. Since no direct hybridization to the band states exists, these peaks are sharper than the corresponding ones in $D_{e\sigma}(\omega)$, i.e., the broadening is introduced indirectly via the Coulomb interaction. Rather more interesting is the appearance of a structure at the Fermi energy consisting of two narrow peaks separated by a gap $\Delta \sim 0.36 \approx J_{cf} = 16/(\pi U) \approx 0.34$ for $t_{12} = 0$. As t_{12} increases, this feature and, in particular, the gap prevails, although its size decreases (see insets to figure 5). Note, however, that the gap edges remain symmetric with respect to the Fermi energy, while the spectral weight is larger below the Fermi level as long as $t_{12} < t_{12,c}$. For $t_{12} > t_{12,c}$, a rearrangement of spectral weight from below to above the Fermi energy takes place, while the size of the gap does not change noticeably.

We interpret this structure as a replica of the Kondo resonance induced indirectly by the interactions between the even and odd channels. However, adding or removing electrons in the odd-parity orbital would at least break one 'Kondo bond' in the even-parity channel, i.e., cost an energy $\sim J_{cf}$, explaining the appearance and size of the gap for $t_{12} = 0$. Note that, in contrast to the weak-coupling regime, this explanation connects the gap to the spin rather than to the charge degrees of freedom. As t_{12} increases, the gap becomes smaller because the direct exchange interaction J_{ex} between the impurity sites competes with the Kondo effect, effectively reducing the local moment, which is screened by the band states, and hence the corresponding spin gap. However, we find $\Delta > J_{cf} - J_{ex}$, which would be the naive expectation, because the formation of dynamic spin correlations between the impurities due to J_{ex} introduces a further contribution to Δ. Thus, the gap will always be finite and develops a minimum close to $t_{12,c}$, where $J_{cf} = J_{ex}$. For $t_{12} > t_{12,c}$, the impurities form a non-local spin singlet and the spin gap will scale with J_{ex}, i.e., increase again slowly with increasing t_{12}. An estimate for $t_{12} \geqslant t_{12,c}$ yields $\Delta \sim J_{ex} = 4t_{12}^2/U \approx 0.26$, which is in rough agreement with the numerical value $\Delta \approx 0.16$ obtained from figure 5(c).

4.2.4. Intermediate-coupling regime. Finally, we present the spectral function for $U \approx 4\pi\Delta_0$, i.e., in the intermediate-coupling regime. Note that from the point of view of the

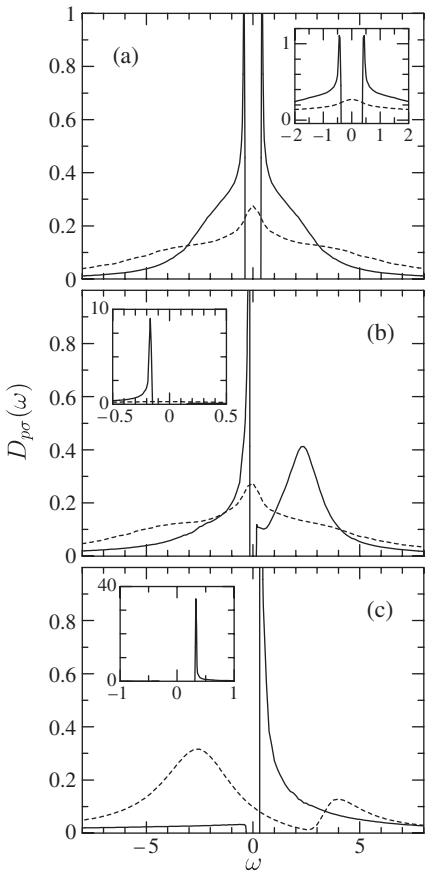

Figure 6. Spectral density of the coupled impurities for the odd-parity orbital $D_{o\sigma}(\omega)$ and for the even-parity orbital $D_{e\sigma}(\omega)$ with (a) $t_{12} = 0$, (b) $t_{12} = 0.5\pi\Delta_0$, and (c) $t_{12} = \pi\Delta_0$ at $U = 5\pi\Delta_0$ and $W = 20\pi\Delta_0$. Dashed lines denote $D_{e\sigma}(\omega)$ calculated with a constant discretization for $N = 58$, $\Delta\varepsilon \approx 0.34\pi\Delta_0$, and $\eta = 0.5\pi\Delta_0$, then deconvolved. Solid lines denote $D_{o\sigma}(\omega)$ calculated with a variable discretization for $N = 118$, $0.01\pi \leqslant \Delta\varepsilon/\Delta_0 \leqslant 1.45\pi$, and a constant broadening $\eta = 0.02\pi\Delta_0$, then deconvolved. Insets: expanded view around the Fermi level $\omega = 0$.

SIAM this value already resides within the 'strong-coupling' regime delimited by $\frac{U}{\pi\Delta_0} = 2$ (the effective hybridization for the even-parity channel is $2\Delta_0$). In figure 6, we show the spectral density calculated with the DDMRG for $t_{12} = 0$, $0.5\pi\Delta_0$, and $\pi\Delta_0$ at $U = 5\pi\Delta_0$. The transition here occurs at $t_{12,c} \sim 0.65\pi\Delta_0$. As already mentioned above, the even-parity spectral density $D_{e\sigma}(\omega)$ below $t_{12,c}$ resembles that of the SIAM. The central peak at $\omega = 0$ starts to become narrower and its spectral weight is increasingly transferred to the high-energy range with increasing U. However, the three-peak structure typical of the strong-coupling regime is not yet fully developed; the Hubbard bands appear only as visible but shallow shoulders around $\omega \sim \pm U/2$. Moreover, in contrast to the SIAM, the central peak here does not fully reach the Friedel limit, its height being slightly lower than $1/\pi$. This behaviour was also seen in previous NRG studies [22] and in the mean-field approach [23], and is connected to the non-local magnetic correlations induced by the RKKY exchange, which is stronger for smaller U. As in the strong-coupling regime, $D_{e\sigma}(\omega)$ hardly changes with increasing t_{12} until $t_{12,c}$ is reached, where a dramatic redistribution of spectral weight connected to the formation

of a non-local singlet due to the direct exchange introduced by t_{12} appears. In particular, as in the strong-coupling regime, the Kondo peak has vanished completely.

The behaviour of the odd-parity channel in figure 6 is also similar to the strong-coupling limit. We again find a gap in the spectrum, which remains symmetric about $\omega = 0$ for all t_{12}, and observe a similar but much more pronounced change in the distribution of spectral weight, as in figure 5. The gap, too, initially decreases until $t_{12,c}$ is reached and then increases again. We believe that the physics behind this behaviour is essentially the same as in the $U \to \infty$ limit, although the energy scales associated with the spin gaps induced by the different exchange mechanism in particular now cannot be written down explicitly. However, we expect them to be larger than in the limit of large U, which is indeed what we observe in figure 6.

5. Conclusion

In this paper, we have presented static and dynamical properties of the two-impurity Anderson model at half filling for vanishing impurity separation. In this limit, the otherwise rather complex model becomes considerably simpler, nevertheless retaining most of its interesting physical aspects. In particular, the competition between different types of magnetic correlations such as Kondo, RKKY and superexchange is preserved. We employ the (dynamical) density-matrix renormalization method to calculate static properties (filling, magnetic correlations) and one-particle spectra. For the latter, we obtain results that are convoluted with a Lorentzian, which we, however, can deconvolute with good accuracy, as demonstrated for the exactly solvable case $U = 0$.

While this model can, in fact, easily be studied by e.g., Wilson's NRG, an evident advantage of the DDMRG is that one obtains an accurate description of spectral features on all energy scales at the cost of the resolution of exponentially small structures. In the NRG, on the other hand, exponentially small scales can be readily resolved, however, at the expense of accuracy at intermediate and high energies. Since we are interested here in describing both the features emerging at intermediate ($\sim J_{\mathrm{RKKY}}$, J_{ex}) and high energy scales (Hubbard bands $\sim U/2$) as well as at a possible small Kondo scale, we feel that the DDMRG is more useful for the present study.

In the weak-coupling regime, $U < 2\pi\,\Delta_0$, we observe a transition between a situation with weakly ferromagnetically coupled impurity spins and a situation with weak antiferromagnetic correlations as function of inter-impurity hopping t_{12}, as is apparent from the behaviour of $\langle \vec{S}_1 \cdot \vec{S}_2 \rangle$ in figure 2(c). From the spectral functions discussed in figure 4, we can furthermore infer that this transition is primarily driven by the charge degrees of freedom in the odd-parity channel of the two-impurity system. For $U > 2\pi\,\Delta_0$, on the other hand, the transition is into a state with rather strong antiferromagnetic correlations. At the same time, the behaviour of the spectral functions, in particular in the odd-parity channel, changes considerably. Although the transition is still accompanied by a change in occupancy in the odd-parity channel, this change is visibly reduced. Furthermore, the gap in the odd-parity spectrum is always pinned to the Fermi energy and is of the size of the typical magnetic exchange interactions, which points to the spin degrees of freedom as the driving force of the transition. Finally, the existence of a Kondo peak in the even-parity spectrum for $t_{12} < t_{12,c}$, which abruptly vanishes for $t_{12} > t_{12,c}$, must be taken as evidence that the transition is in fact driven by the competition between Kondo and direct exchange in this regime. It is quite important to note that the actual transition occurs at the point where $J_{\mathrm{cf}} = J_{\mathrm{ex}}$ and *not* when $T_{\mathrm{K}}(J_{\mathrm{cf}}) = J_{\mathrm{ex}}$, and also that the energy scales appearing in the spectra in figures 5 and 6 are in fact related to these 'intermediate' quantities rather than the actually much smaller Kondo scale.

Of course, the current investigation is restricted to a special limit of the TIAM, namely, that of vanishing impurity separation. The results for this case clearly show that a more thorough investigation of this model is still necessary. In particular, we believe that such an investigation must carefully study the relation between the different energy scales inherent to the problem. The method to study the TIAM should be chosen so that it can at least resolve accurately intermediate, i.e., of the order of the effective exchange interactions, and low energy scales, i.e., of the order of the Kondo scale. Evidently, we cannot expect that any method can handle both regimes equally well when the energy scale of the latter is exponentially small, but we believe that the DDMRG can at least treat the intermediate situation when $T_K \ll J_{ex}$ but is still resolvable with the method.

Acknowledgments

We thank F Gebhard and E Jeckelmann for useful discussions. This work was supported in part by the Deutsch Forschungsgemeinschaft through the collaborative research centre SFB 602. Part of the computations were carried out at the Norddeutsche Verbund f¨ur Hoch- und Höchstleistungsrechnen.

References

[1] Hewson A C 1993 *The Kondo Problem to Heavy Fermions* (Cambridge: Cambridge University Press)
[2] Doniach S 1977 *Physica* B **91** 231
[3] Jeong H, Chang A M and Melloch M R 2001 *Science* **293** 2221
[4] Tsay Y C and Klein M W 1973 *Phys. Rev.* B **7** 352
[5] Jayaprakash C, Krishna-murthy H R and Wilkins J W 1982 *J. Appl. Phys.* **53** 2142
[6] Chakravarty S and Hirsch J E 1982 *Phys. Rev.* B **25** 3273
[7] Jones B A, Kotliar B G and Millis A J 1989 *Phys. Rev.* B **39** 3415
[8] Saso T 1991 *Phys. Rev.* B **44** R450
Saso T and Kato H 1992 *Prog. Theor. Phys.* **87** 331
[9] Andreani L C and Beck H 1993 *Phys. Rev.* B **48** 7322
[10] Schiller A and Zevin V 1993 *Phys. Rev.* B **47** 14297
[11] Santoro G E and Giuliani G F 1994 *Phys. Rev.* B **49** 6746
[12] Klein W, Xianlong G and Ji L 1999 *Phys. Rev.* B **60** 15492
[13] Büsser C A, Anda E V, Lima A L, Davidovich M A and Chiappe G 2000 *Phys. Rev.* B **62** 9907
[14] Ivanov T I 2000 *Phys. Rev.* B **62** 12577
[15] Neto A M J C and Lagos R E 2002 *Physica* B **312/313** 176
[16] Aguado R and Langreth D C 2003 *Phys. Rev.* B **67** 245307
[17] Jayaprakash C, Krishna-murthy H R and Wilkins J W 1981 *Phys. Rev. Lett.* **47** 737
[18] Fye R M, Hirsch J E and Scalapino D J 1987 *Phys. Rev.* B **35** 4901
Fye R M and Hirsch J E 1989 *Phys. Rev.* B **40** 4780
Fye R M 1994 *Phys. Rev. Lett.* **72** 916
[19] Jones B A and Varma C M 1987 *Phys. Rev. Lett.* **58** 843
Jones B A, Varma C M and Wilkins J W 1988 *Phys. Rev. Lett.* **61** 125
Jones B A and Varma C M 1989 *Phys. Rev.* B **40** 324
[20] Affleck I and Ludwig A W W 1992 *Phys. Rev. Lett.* **68** 1046
Affleck I, Ludwig A W W and Jones B A 1995 *Phys. Rev.* B **52** 9528
[21] Ingersent K, Jones B A and Wilkins J W 1992 *Phys. Rev. Lett.* **69** 2594
[22] Sakai O and Shimizu Y 1992 *J. Phys. Soc. Japan* **61** 2333
[23] Sire C, Varma C M and Krishnamurthy H R 1993 *Phys. Rev.* B **48** 13833
[24] Andreani L C and Beck H 1993 *J. Appl. Phys.* **70** 6628
[25] Gan J 1995 *Phys. Rev. Lett.* **74** 2583
Gan J 1995 *Phys. Rev.* B **51** 8287
[26] Georges A and Sengupta A M 1995 *Phys. Rev. Lett.* **74** 2808
[27] Silva J B, Lima W L C, Oliveira W C, Mello J L N, Oliveira L N and Wilkins J W 1996 *Phys. Rev. Lett.* **76** 275

[28] Hallberg K and Egger R 1997 *Phys. Rev.* B **55** R8646
[29] Schlottmann P 1998 *Phys. Rev. Lett.* **80** 4975
[30] Izumida W and Sakai O 2000 *Phys. Rev.* B **62** 10260
[31] Aono T and Eto M 2001 *Phys. Rev.* B **63** 125327
Aono T and Eto M 2001 *Phys. Rev.* B **64** 073307
[32] Vojta M, Bulla R and Hofstetter W 2003 *Phys. Rev.* B **65** 140405(R)
[33] Allub R 2003 *Phys. Rev.* B **67** 144416
[34] Campo V L Jr and Oliveira L N 2004 *Phys. Rev.* B **70** 153401
[35] Jeckelmann E 2002 *Phys. Rev.* B **66** 045114
[36] Nishimoto S and Jeckelmann E 2004 *J. Phys.: Condens. Matter* **16** 613
[37] Raas C, Uhrig G S and Anders F B 2004 *Phys. Rev.* B **69** 041102(R)
[38] Wilson K G 1975 *Rev. Mod. Phys.* **47** 773
[39] White S R 1992 *Phys. Rev. Lett.* **69** 2863
White S R 1993 *Phys. Rev.* B **48** 10345
[40] Peschel I, Wang X, Kaulke M and Hallberg K (ed) 1999 *Density-Matrix Renormalization* (Berlin: Springer)